Spatial regulation of organelle release from myosin V transport by p21-activated kinases

Richard G. Yau,[1,3]* Sara Wong,[1,3]* and Lois S. Weisman[1,2,3]

[1]Cellular and Molecular Biology Program, [2]Department of Cellular and Developmental Biology, and [3]Life Sciences Institute, University of Michigan, Ann Arbor, Michigan 48109

Correct positioning of organelles is essential to eukaryotic cells. Molecular motors transport organelles to their proper destinations, yet little is known about the pathways that define these destinations. In *Saccharomyces cerevisiae*, the myosin V motor Myo2 binds the vacuole-specific adapter Vac17 to attach to the vacuole/lysosome and initiate transport. After arrival in the bud, Myo2 releases the vacuole, and Vac17 is degraded. However, the mechanisms that spatially regulate this release were not established. In this study, we report that the bud cortex is a landmark that signals a successful delivery of the vacuole to the bud. We demonstrate that upon arrival at the bud cortex, Vac17 is phosphorylated by Cla4. Cla4-dependent phosphorylation is required for the ubiquitylation and subsequent degradation of Vac17 and the release of the vacuole from Myo2. Our study reveals a critical step in the spatial regulation of myosin V–dependent organelle transport and may reveal common mechanisms for how molecular motors accurately deposit cargoes at the correct locations.

Introduction

Myosin V motors transport organelles to their correct intracellular locations. Transport initiates when myosin V binds cargo-specific adapters and attaches to organelles (Weisman, 2006; Westermann, 2014; Knoblach and Rachubinski, 2016). Upon arrival at their correct locations, organelles detach from myosin V, thereby terminating transport. The molecular mechanisms that signal the arrival of organelles at their correct locations remain unclear.

At the beginning of the cell cycle in *Saccharomyces cerevisiae*, the myosin V motor Myo2 binds the vacuole adapter Vac17 and transports a portion of the mother vacuole into the bud (Ishikawa et al., 2003; Peng and Weisman, 2008; Eves et al., 2012). In the bud, the vacuole is released from Myo2, and Vac17 is degraded (Tang et al., 2003). Degradation of Vac17 requires phosphorylated Vac17-T240, which recruits the E3 ubiquitin ligase Dma1. Dma1 then ubiquitylates Vac17, targeting Vac17 for degradation by the proteasome (Yau et al., 2014). Late in the cell cycle, Myo2 transports secretory vesicles, but not the vacuole, to the mother-bud neck (Govindan et al., 1995; Pruyne et al., 1998; Schott et al., 1999). In mutants defective in the degradation of Vac17, the vacuole remains attached to Myo2 and is inappropriately transported to the mother-bud neck late in the cell cycle (Tang et al., 2003; Yau et al., 2014).

In yeast, the p21-activated kinases (PAKs) Cla4 and Ste20 localize to the bud cortex and regulate several cell cycle–related processes, including actin cytoskeleton polarization, septin ring assembly, and cytokinesis (Cvrcková et al., 1995; Peter et al., 1996; Kumar et al., 2009; Boyce and Andrianopoulos, 2011). Moreover, it was proposed that PAKs indirectly regulate vacuole inheritance via Lte1, a Cla4-activated guanine nucleotide exchange factor (Bartholomew and Hardy, 2009).

In this study, we report that PAKs directly phosphorylate Vac17 to signal the arrival of the vacuole at its correct location. We show that before the termination of vacuole inheritance, the vacuole extends to the bud cortex, where Vac17 colocalizes with Cla4. In contrast to a previous study, we find that neither degradation of Vac17 nor termination of vacuole transport require Lte1 (Bartholomew and Hardy, 2009). Instead, Cla4 directly phosphorylates Vac17-S222. This phosphorylation event is required for Dma1-dependent ubiquitylation and degradation of Vac17 as well as the release of the vacuole from Myo2. Moreover, in a Vac17 mutant that cannot be phosphorylated at S222, the vacuole remains attached to the bud cortex, which suggests that this is the intracellular location where Cla4 phosphorylates Vac17. Collectively, these studies suggest that at the bud cortex, Cla4 initiates a signaling cascade to regulate the ubiquitylation of Vac17 and complete the termination of vacuole transport, thereby ensuring that the vacuole is deposited at the correct intracellular location.

---

*R.G. Yau and S. Wong contributed equally to this paper.

Correspondence to Lois S. Weisman: lweisman@umich.edu

Abbreviation used: PAK, p21-activated kinase.

Results and discussion

PAKs are required for Vac17 degradation and termination of vacuole transport

A previous study suggested that Lte1 regulates Vac17 degradation (Bartholomew and Hardy, 2009). However, it was unknown whether Lte1 directly regulates the termination of vacuole transport. To investigate whether Lte1 acts in this pathway, we tested the *lte1Δ* mutant for the stabilization of Vac17-GFP and the mislocalization of Vac17-GFP and the vacuole to the mother-bud neck in large-budded cells. However, these defects were not observed in the absence of *LTE1* (Fig. S1, A–C). We then measured the impact of PAK function on vacuole inheritance. Vac17 levels were not detectably elevated in the *cla4Δ* or *ste20Δ* mutants. Furthermore, only a partial defect in the termination of vacuole was observed, whereby Vac17-GFP and the vacuole colocalized at the bud tip and mother-bud neck in some large-budded cells. These phenotypes were more prominent in the *cla4Δ* mutant (Fig. S1 D–F).

Because PAKs are functionally redundant and synthetically lethal, we performed experiments in the *cla4^{ts} ste20Δ* double mutant (Cvrcková et al., 1995; Martín et al., 1997; Holly and Blumer, 1999; Tatebayashi et al., 2006). At 24°C, the levels of Vac17 in the *ste20Δ cla4^{ts}* mutant were similar to wild-type levels. In contrast, at 37°C, Vac17 was stabilized and exhibited an increase in electrophoretic mobility, which suggests a loss of posttranslational modifications (Fig. 1 A). In the *cla4^{ts} ste20Δ* mutant at 24°C, there was partial mislocalization of the vacuole with Vac17-GFP, consistent with the finding that the *ste20Δ* mutant has a minor defect in the termination of vacuole transport (Fig. S1, D–F). In large-budded *cla4^{ts} ste20Δ* cells at 37°C, Vac17-GFP and the vacuole accumulated at the mother-bud neck, similar to the *dma1Δ dma2Δ* mutant (Yau et al., 2014). Intriguingly, we also observed Vac17 and the vacuole at a new aberrant location: the bud tip. This raises the possibility that the bud cortex is the landmark where Myo2 releases the vacuole. In addition, Vac17-GFP and the vacuole mislocalized to the cell cortex at a site adjacent to the mother-bud neck (a location on the cortex between the bud tip and mother-bud neck). This localization had not been previously reported for the vacuole or Myo2 (Fig. 1, B and C). The mislocalization of the vacuole to this site may be caused by defects in the organization of the actin cytoskeleton in the *cla4^{ts} ste20Δ* mutant (Holly and Blumer, 1999).

To test whether PAK function is required to detach the vacuole from Myo2, we analyzed colocalization between Myo2-Venus and the vacuole in large-budded cells. In wild-type cells at 24°C and 37°C, the vacuole detached correctly and did not colocalize with Myo2-Venus. In the *cla4^{ts} ste20Δ* mutant at 24°C, there was a modest defect in the termination of vacuole transport. At 37°C in the *cla4^{ts} ste20Δ* mutant, there was a strong defect in the detachment of the vacuole from Myo2-Venus. The vacuole colocalized with Myo2-Venus at the bud tip, mother-bud neck, and adjacent to the mother-bud neck (Fig. 1, D and E). These observations suggest that PAK-dependent signaling regulates Vac17 degradation, the release of the vacuole from Myo2, and the termination of vacuole transport.

Cla4 phosphorylates Vac17 in vivo and in vitro

That PAKs regulate Vac17 levels independently of Lte1 suggests that PAKs directly target Vac17. In support of this hypothesis, recombinant GST-Cla4, but not GST alone, binds Vac17-TAP

from cell extracts (Fig. 2 A). Cla4 phosphorylates serines within the consensus motif RxS (Wu et al., 1996; Versele and Thorner, 2004; Mok et al., 2010). Interestingly, Vac17-S222 matches this motif, Vac17-R$_{220}$LS$_{222}$, and is required for Vac17 degradation and the termination of vacuole transport (Yau et al., 2014). To determine whether Vac17-S222 is a Cla4 phosphorylation site, we generated a phosphospecific antibody for Vac17-pS222 and tested it against Vac17-GFP and *vac17-S222A-GFP* expressed in *vac17Δ* or *dma1Δ dma2Δ vac17Δ* mutants. Deletion of *DMA1* and *DMA2* stabilizes phosphorylated Vac17, thereby facilitating its detection (Yau et al., 2014). The anti-pS222 antibody recognized Vac17-GFP but not *vac17-S222A-GFP* (Fig. 2 B). Furthermore, this antibody does not recognize dephosphorylated Vac17-GFP, indicated by an increase in electrophoretic mobility, in λ-phosphatase–treated samples (Fig. 2 C). These results demonstrate the specificity of this antibody for Vac17-pS222 and that Vac17-S222 is phosphorylated in vivo.

To test whether PAK activity is required for the phosphorylation of Vac17-S222 in vivo, we analyzed Vac17-S222 phosphorylation in the *cla4^{ts} ste20Δ* mutant. Inactivation of PAK activity reduced phosphorylation of Vac17-S222. This result suggests that PAK activity is required for the phosphorylation of S222 in vivo. Phosphorylation of T240 may have been slightly affected by reduced pS222 or by indirect effects of the *cla4^{ts} ste20Δ* mutant (Fig. 2, D and E).

Because Vac17-S222 matches the Cla4 consensus site, we tested whether Cla4 directly phosphorylates Vac17. We performed in vitro kinase assays using recombinant GST-Cla4 and a 6×HIS-Vac17 (96–355) peptide. Phosphorylation was detected via immunoblotting with the anti-pS222 antibody. GST-Cla4, but not kinase-dead *GST-cla4-K594A,* phosphorylated 6×HIS-Vac17 (96–355) in an ATP-dependent manner. Additionally, the antibody did not recognize products of this reaction if the 6×HIS-*vac17-S222A* (96–355) peptide was used (Fig. 2 F). Collectively, these results demonstrate that Cla4 directly phosphorylates Vac17-S222.

Phosphorylation of Vac17-S222 is required for the termination of vacuole transport

To gain insight into the role of Vac17-pS222, we tested the termination of vacuole transport in cells expressing the nonphosphorylatable *vac17-S222A-GFP* mutant. In large-budded cells, *vac17-S222A-GFP* mislocalized with the vacuole at the mother-bud neck, similar to *vac17-T240A-GFP*. Upon closer analysis, both *vac17* mutants also accumulated with the vacuole at the bud tip in large-budded cells before relocalizing to the mother-bud neck, as seen in the *cla4^{ts} ste20Δ* mutant. In contrast, the vacuole was properly localized in the bud, and no GFP signal was detected in cells expressing Vac17-GFP (Fig. 3, A and B). These results demonstrate that phosphorylation of Vac17-S222 is required to terminate vacuole transport and support the hypothesis that termination of transport initiates at the bud tip. In addition, the localization of Myo2 was not perturbed by the mislocalization of the vacuole (Fig. 3, C–E) or Vac17 (Fig. 3, F–H) in the *vac17-S222A-GFP* and *vac17-T240A-GFP* mutants. This suggests that the trajectory of Myo2 is not dictated by its bound cargoes.

Vac17-pS222 is required for the ubiquitylation of Vac17

The termination of vacuole transport occurs in regulated steps: (A) Vac17-T240 is phosphorylated, (B) Dma1 is recruited to the vacuole, (C) Dma1 ubiquitylates Vac17, and (D) Vac17 is
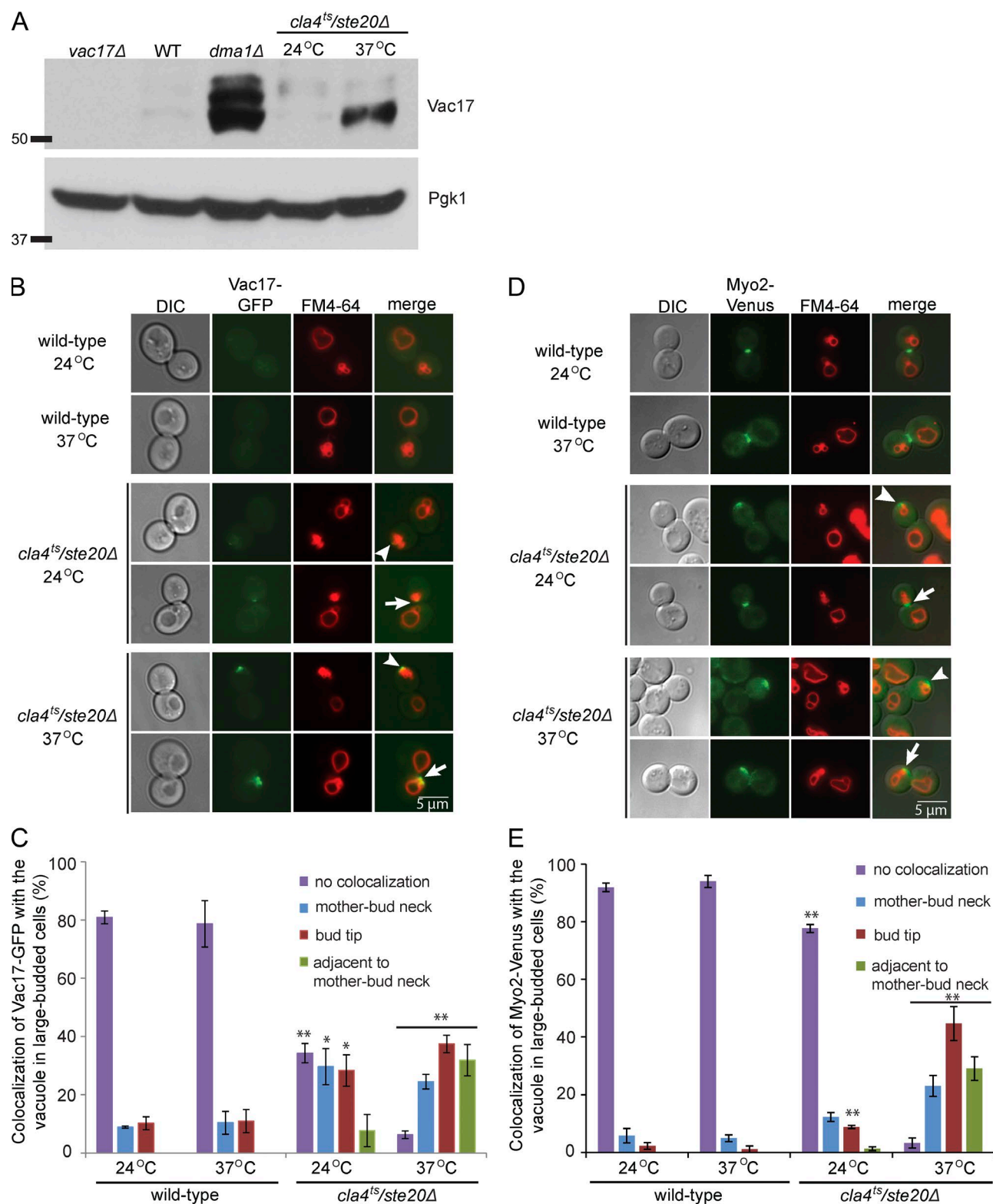
Figure 1. **PAKs are required for the degradation of Vac17 and the release of the vacuole from Myo2.** (A) Vac17 levels are elevated in *dma1Δ* and *cla4ts ste20Δ* mutants. The *cla4ts ste20Δ* mutant was grown at either 24°C or shifted to 37°C for 3 h before lysis. Pgk1 was used as a loading control. Molecular mass is shown in kilodaltons. (B–E) Loss of PAK function results in mislocalization of the vacuole (FM4-64; B and D) and accumulation of Vac17-GFP (B) at the bud tip (arrowheads) or mother-bud neck (arrows). Wild-type (WT) and *cla4ts ste20Δ* cells were transformed with Vac17-GFP (B) or Myo2-Venus (D). After FM4-64 labeling, cells were chased either at 24°C for 3 h or 24°C for 90 min and then 37°C for 90 min before imaging. DIC, differential interference contrast. (C and E) Quantification of >35 large-budded cells per condition per *n*. Error bars indicate SEM. *n* = 3. *, P < 0.05; **, P < 0.01; two-tailed Student's *t* test.

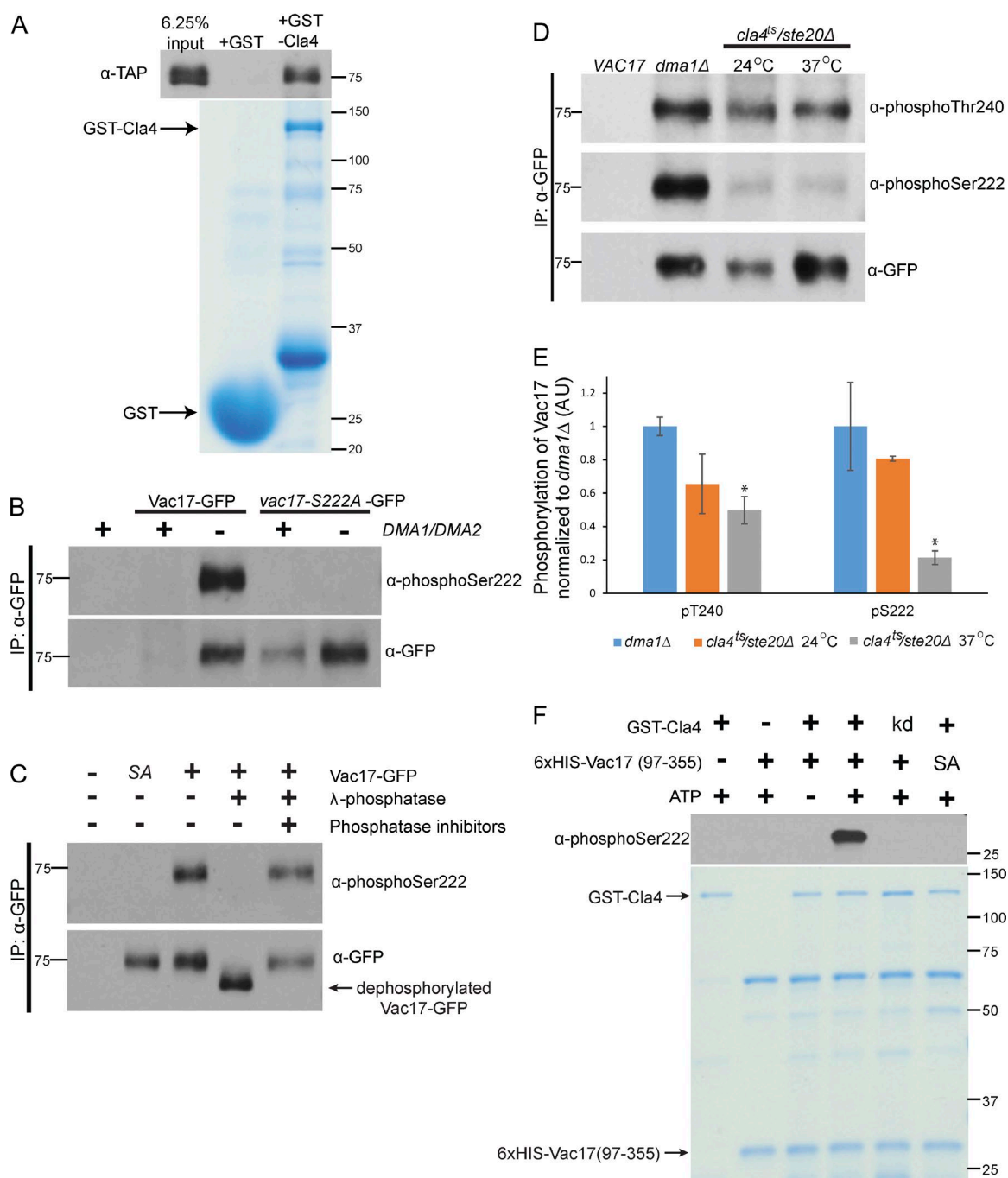Figure 2. **Cla4 binds and phosphorylates Vac17.** (A) Purified recombinant GST-Cla4 but not GST alone binds Vac17-TAP from *dma1Δ dma2Δ VAC17-TAP* lysates. (B) The anti-pS222 antibody recognizes wild-type Vac17-GFP but not the *vac17-S222A-GFP* mutant. (C) λ-Phosphatase treatment causes an increase in the electrophoretic mobility of Vac17-GFP and ablates detection by the anti-pS222 antibody. (D) Inactivation of PAKs decreases the phosphorylation of Vac17-S222 and to a lesser extent, Vac17-T240. Vac17 phosphorylation was monitored using anti-pS222 or anti-pT240 antibodies in the *cla4ts ste20Δ* mutant transformed with Vac17-GFP. Cells were grown at 24°C or shifted to 37°C for 3 h before immunoprecipitation (IP) of Vac17-GFP using anti-GFP antibodies. As a positive control, Vac17-GFP immunoprecipitated from a *dma1Δ* mutant was phosphorylated at both sites. (E) Levels of pT240 or pS222 were normalized to GFP, and those ratios were normalized to *dma1Δ*. Error bars indicate SEM. $n = 2$. *, $P < 0.05$; two-tailed Student's *t* test. AU, arbitrary unit. (F) 6×HIS-Vac17 (96–355) but not 6×HIS-*vac17-S222A* (96–355) was phosphorylated by Cla4 but not the kinase-dead *cla4-K594A* mutant nor in the absence of ATP. Phosphorylation was analyzed via immunoblotting with the anti-pS222 antibody. *SA* indicates the *vac17-S222A-GFP* mutant, and kd indicates the Cla4 kinase-dead mutant. Molecular mass is indicated in kilodaltons.

degraded to release the vacuole from Myo2 (Yau et al., 2014). Because Vac17-S222 is required for the termination of vacuole transport, we tested whether Vac17-S222 functions at any of these known steps. Immunoblotting with the anti-pT240 antibody demonstrated that Vac17-GFP and *vac17-S222A*-

GFP but not *vac17-T240A-GFP* were phosphorylated at T240. Conversely, Vac17-GFP and *vac17-T240A-GFP* but not *vac17-S222A-GFP* were phosphorylated at S222 (Fig. 4, A and B). These results demonstrate that phosphorylation of Vac17-S222 and Vac17-T240 occur independently of each other and are
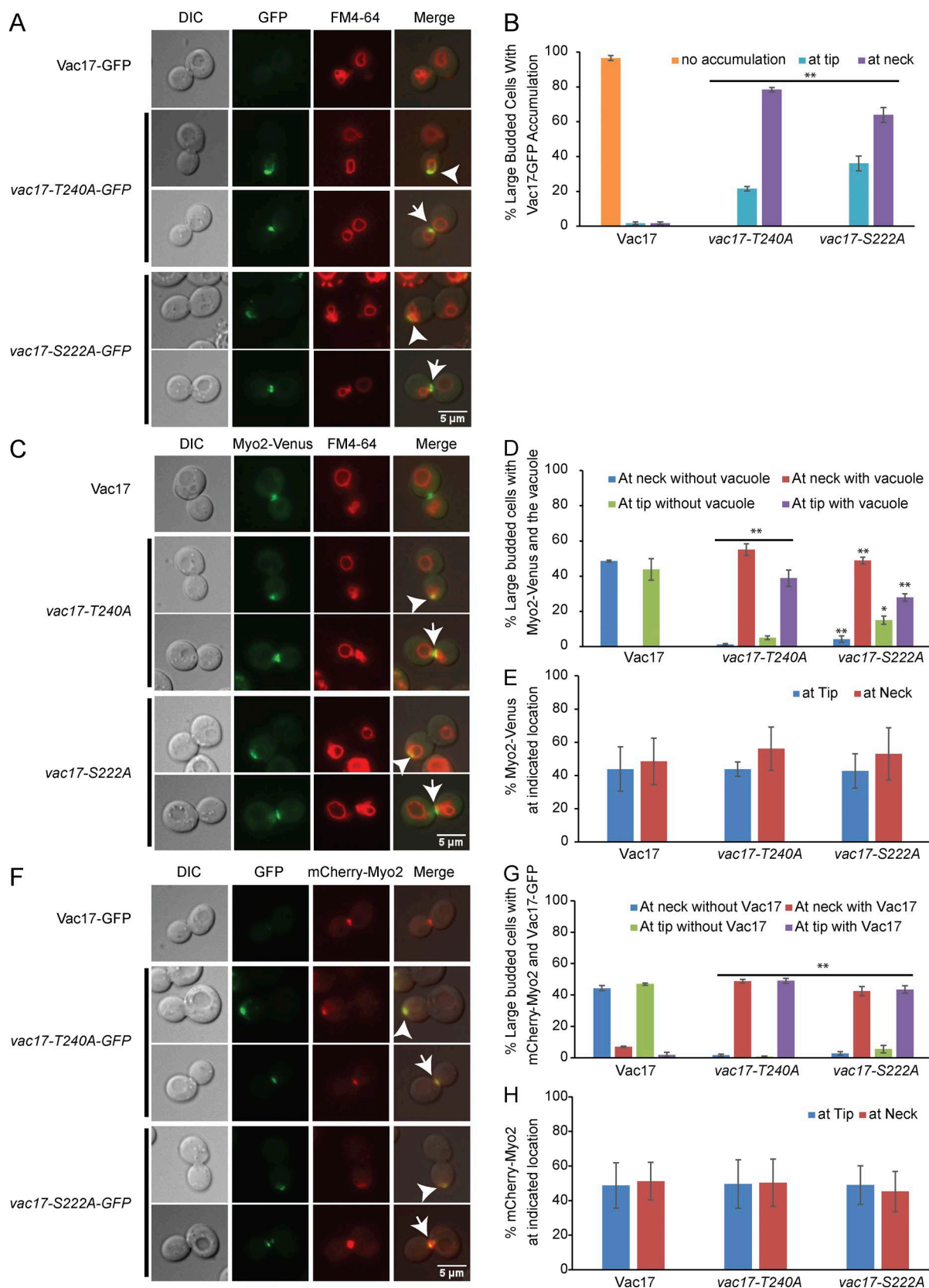
Figure 3. **Termination of vacuole transport initiates at the bud cortex.** (A, C, and F) Fluorescence microscopy of a *vac17Δ* strain transformed with plasmids encoding GFP-tagged *VAC17* or *vac17* point mutants with or without mCherry- or Venus-tagged Myo2. (A) *vac17-S222A-GFP* and *vac17-T240A-GFP* resulted in mislocalization of the vacuole (FM4-64) to the bud tip (arrowheads) or mother-bud neck (arrows). (B) Quantification of >30 large-budded cells per strain per *n*. (C) Vacuoles colocalize with Myo2-Venus at the bud tip (arrowheads) or mother-bud neck (arrows) in cells expressing *vac17-S222A* or *vac17-T240A*. (D) Quantification of >40 large-budded cells per strain per *n* for the colocalization of Myo2 and the vacuole. (E) Quantification of >40

consistent with the trend of reduced Vac17-S222 phosphorylation during PAK inactivation (Fig. 2, D and E).

To determine whether Vac17-S222 is required for the recruitment of Dma1, we tested the localization of Dma1 during vacuole transport. We observed Dma1-3×GFP at the bud vacuole in the majority of small-budded cells expressing *vac17-S222A*, similar to wild type. This contrasts with the *vac17-T240A* mutant, which is defective in Dma1 recruitment (Fig. 4, C and D). That Dma1 is recruited to the vacuole in cells expressing *vac17-S222A* is consistent with the observation that *vac17-S222A* does not impair phosphorylation of Vac17-T240.

Because recruitment of Dma1 to the vacuole is unperturbed in the *vac17-S222A* mutant, we predicted that *vac17-S222A* would be ubiquitylated similarly to wild type. To test this hypothesis, *VAC17-GFP* or *vac17-S222A-GFP* were overexpressed in *vac17Δ* cells along with *myo2-D1297N*, a mutant defective in binding Vac17 (Ishikawa et al., 2003). The *myo2-D1297N* mutant was included because overexpression of *vac17-S222A-GFP* likely interfered with the ability of Myo2 to transport essential cargoes (Eves et al., 2012) and did not yield viable cells. Cells were also transformed with a plasmid encoding Myc-ubiquitin driven under an inducible promoter. GFP-tagged Vac17 constructs were immunoprecipitated, and ubiquitylation was detected via immunoblotting with anti-Myc antibodies. Surprisingly, *vac17-S222A-GFP* was not ubiquitylated in vivo (Fig. 4 E). These findings indicate that phosphorylation of Vac17-S222 is not required for the recruitment of Dma1 to the vacuole transport complex, but must occur before Dma1 can ubiquitylate Vac17. Thus, phosphorylation of Vac17-S222 may spatially regulate the termination of vacuole transport through regulating Dma1 activity.

Cla4 signaling at the bud cortex initiates the release of the vacuole from Myo2

Cla4 localizes to the bud cortex of small-budded cells and later appears as a punctum on the vacuole in large-budded cells (Bartholomew and Hardy, 2009). To further analyze Cla4 localization in relation to vacuole transport, we performed time-lapse microscopy of cells expressing Cla4-3×GFP and the vacuole marker Vph1-mCherry. In small-budded cells, Cla4-3×GFP appears on the bud cortex, as previously described (Bartholomew and Hardy, 2009). A portion of the vacuole then enters the bud and extends to the bud cortex, where it colocalizes with Cla4. A punctum of Cla4 then moves onto the vacuole (Fig. S2). These observations suggest that arrival of the vacuole at the bud cortex initiates Cla4 signaling on the vacuole. Additionally, Cla4 activity is required for proper unloading of the vacuole from Myo2. In a wild-type cell, Vac17-GFP is barely visible, and the vacuole is in the center of the cell (Video 1). In the nonphosphorylatable *vac17-S222A* mutant, the vacuole and *vac17-S222A-GFP* persist at the bud tip and eventually move from the bud tip to the mother-bud neck (Video 2). In further support that Cla4 is acting at the cortex, we find that the Cla4 homologue Ste20 partially substitutes for Cla4 (Fig. S1, D and E), yet Ste20 is solely at the bud cortex (Peter et al., 1996; Takahashi and Pryciak, 2007). Collectively, these findings suggest that PAKs signal the release of the vacuole from Myo2 at the bud cortex.

To determine whether Cla4 and Vac17 colocalize at the bud cortex, we analyzed the localization of Cla4-tdTomato and Vac17-GFP expressed in the *cla4Δ vac17Δ* mutant via synchronization with α-factor and imaging at 10-min intervals. At 50 min after release, Cla4-tdTomato and Vac17-GFP colocalized at the bud cortex. At 80 min after release, Vac17-GFP was no longer detected. This observation is consistent with the degradation of Vac17 (Tang et al., 2003; Peng and Weisman, 2008). Additionally, even though Vac17 was degraded, a punctum of Cla4 was observed on the vacuole as previously described (Figs. 5 A and S3; Bartholomew and Hardy, 2009). We then analyzed the dynamics of Cla4-tdTomato and *vac17-S222A-GFP*. In contrast to wild type, Cla4 and Vac17 colocalized 60 min after release. At 80 min after release, *vac17-S222A-GFP* accumulated with the vacuole at the bud tip, whereas a punctum of Cla4 localized to a different area of the vacuole. At 120 min after release, *vac17-S222A-GFP* mislocalized with the vacuole at the mother-bud neck (Figs. 5 B and S3). These data suggest that a transient interaction between Cla4 and Vac17 at the leading edge of the vacuole occurs after the vacuole reaches the bud cortex. Moreover, when Cla4 fails to phosphorylate *vac17-S222A*, *vac17-S222A* and the vacuole persist at the bud cortex before mislocalizing to the mother-bud neck (Fig. 5 B and Video 2). These data suggest that Cla4 phosphorylates Vac17-S222 upon arrival of the vacuole at the bud cortex, triggering Vac17 degradation and release of the vacuole from Myo2.

We report here that Cla4 provides spatial control for the termination of vacuole transport and that the bud cortex is the landmark that signals the successful delivery of a myosin V cargo to its correct intracellular location. We show that contact between Cla4 and Vac17 at the bud cortex (Fig. S2) initiates the termination of vacuole transport. Cla4 directly regulates Vac17 degradation via phosphorylating Vac17-S222 (Fig. 2). Intriguingly, phosphorylation by Cla4 is required for the ubiquitylation and degradation of Vac17 (Figs. 3 and 4) but not for the recruitment of Dma1 to the vacuole (Fig. 4). Collectively, our study suggests that once the vacuole reaches the bud cortex, Cla4 initiates a signaling cascade that activates Dma1 to ubiquitylate Vac17 and complete the termination of vacuole inheritance. Vac17-S222 phosphorylation may change the conformation of Vac17 so that it is amenable for Dma1-dependent ubiquitylation or recruit a binding partner that activates Dma1 (Fig. 5 C). These roles for Cla4 in Myo2 transport suggest a direct molecular link between cell polarity factors and the positioning of organelles. Our study reveals that myosin V relies on a spatially regulated signaling cascade to successfully transport cargoes to their correct destinations.

Materials and methods

Yeast strains, plasmids, and media

Unless specified, yeast cultures were grown in yeast extract peptone dextrose containing 1% yeast extract, 2% peptone, and 2% dextrose or in synthetic complete media lacking the indicated amino acids at 24°C. Yeast strains and plasmids are listed in Tables S1 and S2, respectively.

large-budded cells per strain per *n* for the localization of Myo2. (F) *vac17-S222A-GFP* and *vac17-T240A-GFP* colocalize with mCherry-Myo2 at the bud tip (arrowheads) or mother-bud neck (arrows). DIC, differential interference contrast. (G) Quantification of >58 large-budded cells per strain per *n* for the colocalization of Myo2 and Vac17. (H) Quantification of >58 large-budded cells per strain per experiment for the localization of Myo2. Error bars indicate SEM. *n* = 3. *, P < 0.05; **, P < 0.01; two-tailed Student's *t* test.
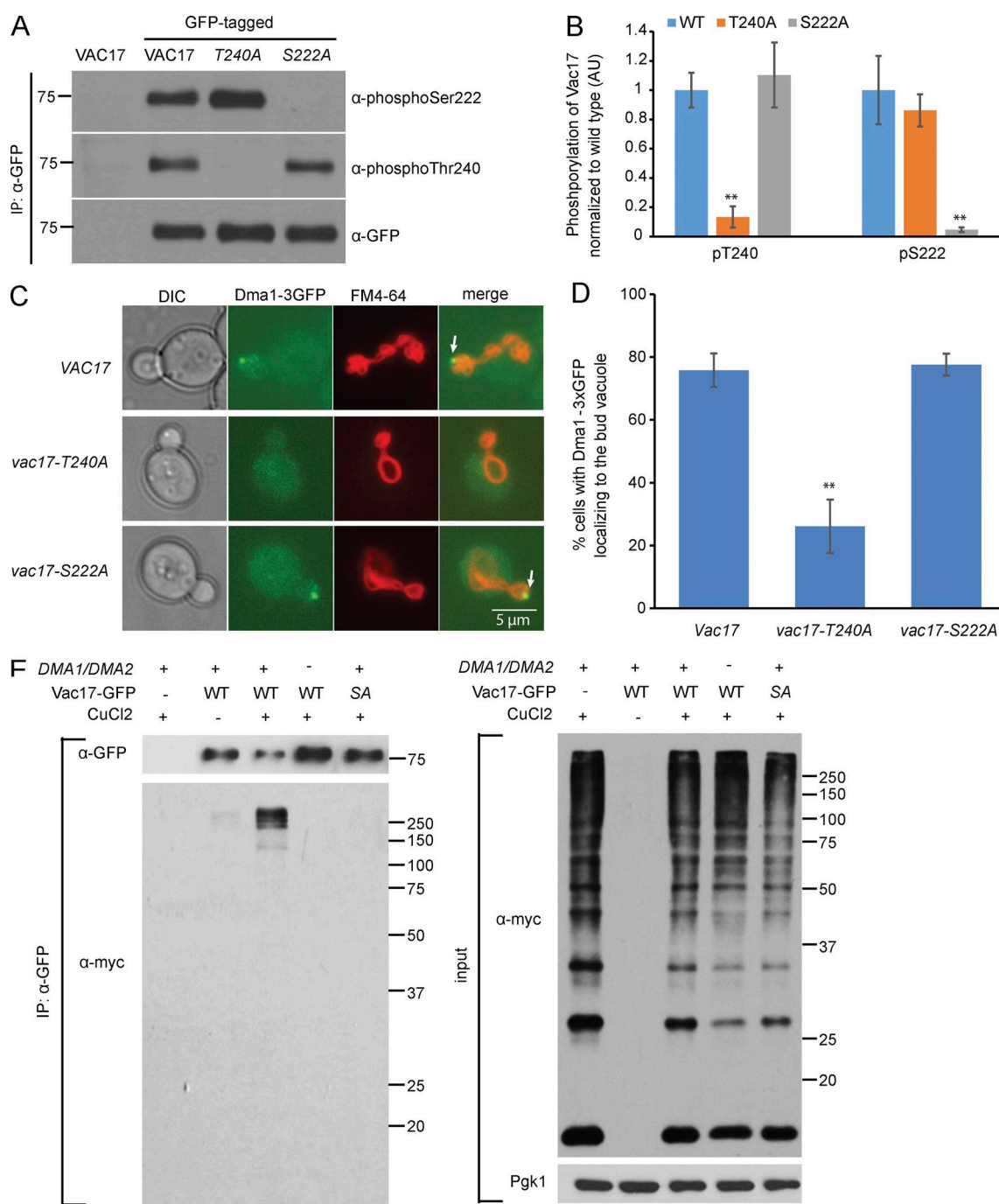
Figure 4. **Vac17-S222 is required for the ubiquitylation of Vac17.** (A) Phosphorylation of Vac17-S222 and Vac17-T240 are independent of each other. (B) Levels of pT240 or pS222 were normalized to GFP, and those ratios were normalized to wild type (WT). AU, arbitrary unit. (C) Dma1 recruitment to the vacuole (FM4-64; arrows) does not require Vac17-S222. Wild-type *VAC17* or *vac17* point mutants were expressed from plasmids in a *DMA-3×GFP vac17Δ* strain. DIC, differential interference contrast. (D) Quantification of >21 cells per strain per *n*. Error bars indicate SEM. *n* = 3. **, P < 0.01; two-tailed Student's *t* test. (E) The *vac17-S222A* mutant is not ubiquitylated in vivo. *vac17Δ* and *dma1Δ dma2Δ vac17Δ* cells were cotransformed with a plasmid encoding myc-ubiquitin under a copper-inducible promoter and plasmids encoding GFP-tagged *VAC17* or *vac17-S222A*. GFP-tagged proteins were immunoprecipitated (IP) using anti-GFP antibodies. Ubiquitylation detected via immunoblotting with anti-myc antibody. Pgk1 was used as a loading control. *SA* indicates the *vac17-S222A-GFP* mutant. Molecular mass is shown in kilodaltons.

Western blot analysis

Cells were harvested and lysed in 1 ml 0.2 M NaOH and 0.2% β-mercaptoethanol. Proteins were precipitated via the addition of 100 µl TCA and centrifuged at 12,000 rpm. Proteins were resuspended in 120 µl 2× SDS sample buffer followed by the addition of 30 µl of 1 M Tris base, pH ~11. Samples were heated at 75°C and analyzed via immunoblot (Peng and Weisman, 2008). For immunoblot analyses, mouse anti-GFP (1:1,000; Roche), rabbit anti-TAP (1:1,000; Thermo Fisher Scientific), mouse anti-Pgk1 (1:10,000; Invitrogen), sheep anti-Vac17 (1:1,000; custom made; 21st Century Biochemicals), rabbit anti–phospho-Thr240 (1:2,500; custom made; 21st Century Biochemicals), and rabbit anti–phospho-Ser222 (1:2,500; custom
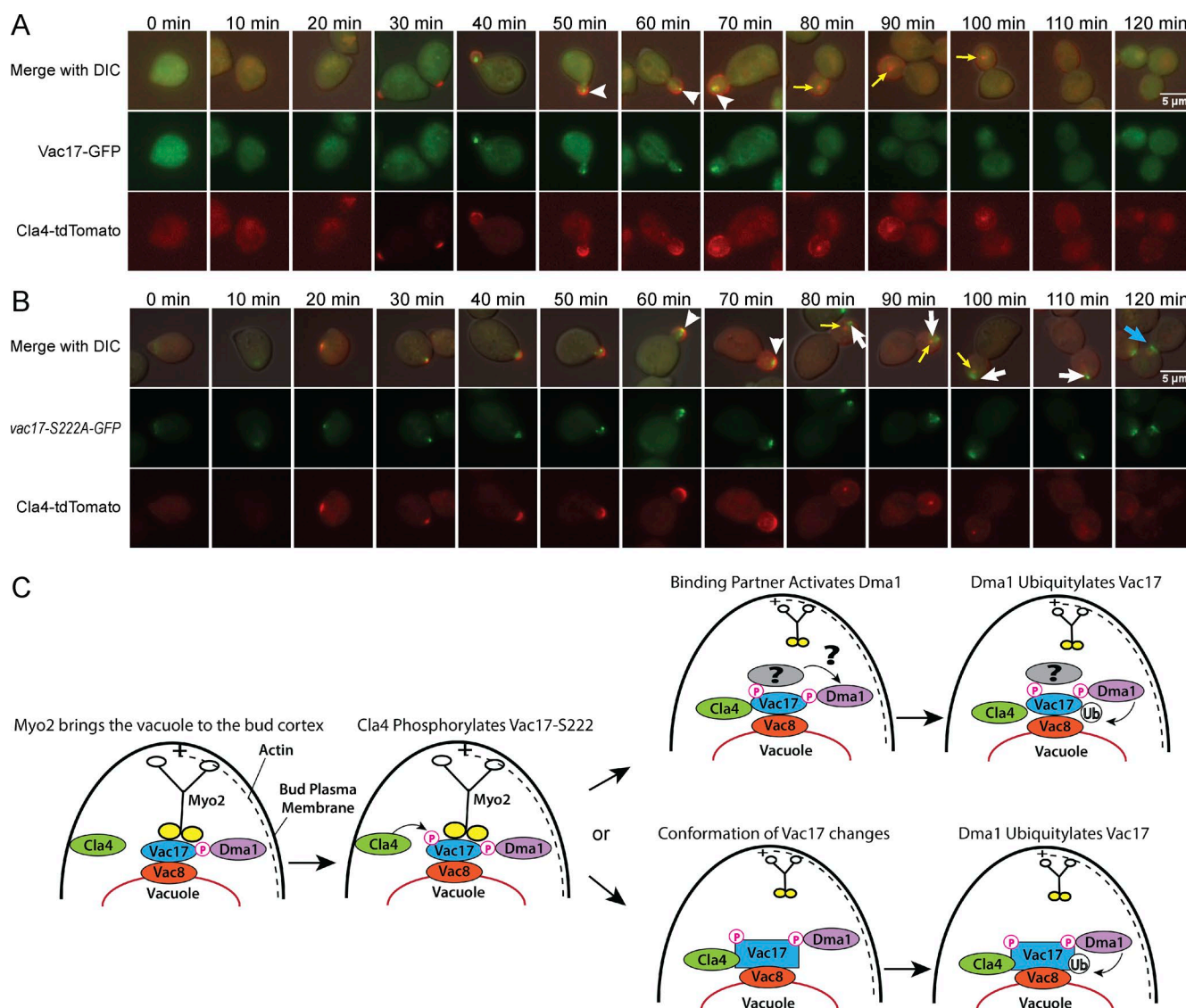
Figure 5. **The initiation of Cla4 signaling at the vacuole occurs at the bud cortex.** (A and B) *cla4Δ vac17Δ* mutant transformed with Cla4-tdTomato and either Vac17-GFP or *vac17-S222A-GFP* plasmids. Cells synchronized with α-factor were imaged every 10 min after release. Representative images from >25 cells per strain per time point per *n*. *n* = 3. DIC, differential interference contrast. (A) Cla4-tdTomato colocalized with Vac17-GFP at the bud cortex (arrowheads). After Vac17-GFP was no longer detected, Cla4-tdTomato was localized away from the cortex (yellow arrows). (B) Cla4-tdTomato and *vac17-S222A-GFP* colocalized at the bud cortex (arrowheads). *vac17-S222A-GFP* persisted at the bud tip (white arrows) and later at the mother-bud neck (blue arrow) after Cla4-tdTomato localized to a different location on the vacuole (yellow arrows). (C) Model showing how Myo2 brings a portion of the vacuole and Vac17 to the bud cortex where Cla4 phosphorylates Vac17. A punctum of Cla4 then moves onto the vacuole. Cla4-dependent phosphorylation of Vac17 may either recruit a downstream binding partner or change the conformation of Vac17 to facilitate Dma1-dependent ubiquitylation of Vac17 and thus the termination of vacuole transport.

made; 21st Century Biochemicals) antibodies were used (see the Antibody preparation section).

Immunoprecipitation experiments

Cells were lysed and proteins were precipitated as described in the Western blot analysis section. Precipitated proteins were washed with acetone, dried, and resuspended in 200 µl urea buffer (6 M urea, 1% SDS, and 50 mM Tris-HCl, pH 7.5) and then were heated at 75°C for 10 min. 1.8 ml TWIP buffer (50 mM Tris-HCl, pH 7.5, 150 mM NaCl, 0.5% Tween-20, and 0.1 mM EDTA) containing 1 mM Na_3VO_4, and 1× protease inhibitor cocktail (Sigma-Aldrich) was added to the resuspended protein and centrifuged. 4 µg of mouse anti-GFP antibodies (Roche) were added to the supernatant and incubated with agitation at 4°C overnight. Immune complexes were harvested via the addition of protein G beads, which were subsequently collected via centrifugation and washed with TWIP buffer. Bound proteins were analyzed via immunoblot.

For dephosphorylation of Vac17-GFP, protein G beads were collected via centrifugation and washed three times with TWIP buffer without EDTA. The beads were resuspended in 1× λ-phosphatase buffer containing 1× protease inhibitor cocktail (Sigma-Aldrich) and 10 mM $MnCl_2$. Either water, λ-phosphatase (400 U; New England Biolabs, Inc.) or λ-phosphatase plus phosphatase inhibitors (100 mM NaF, 10 mM Na_3VO_4, 50 mM EDTA, 20 mM β-glycerophosphate, and 20 mM sodium pyrophosphate) were added to the samples. Phosphatase reactions were performed in a volume of 100 µl and incubated at 30°C for 1 h. Reactions were terminated by addition of 50 µl 2× SDS sample buffer and heated at 75°C for 10 min.

Antibody preparation

The anti-pT240 and anti-pS222 phosphospecific antibodies were made by 21st Century Biochemicals. To generate the anti-pT240 antibody, the unmodified peptide Thr240 NP (CKK-Ahx-FDSDQDTIILP-NI-amide) was used for immunodepletion. The immunogens pThr240 NT (CKK-Ahx-FDSDQD[pT]IILPNI-amide) and pThr240 CT (acetyl-FDSDQD[pT]IILPNI-Ahx-KKC-amide) were mixed for both immunization and affinity purification. To generate the anti-pS222 antibody, the unmodified peptide Ser222 NP (C-Ahx-KNRQRLSLTFFDE-amide) was used for immunodepletion. The immunogens pSer222 NT (C-Ahx-KNRQRL[pS]LTFFDE-amid) and pSer222 CT (acetyl-KNRQRL[pS]LTFFDE-Ahx-C-amide) were mixed for both immunization and affinity purification.

To purify Vac17 antibodies, serum was loaded onto a protein A sepharose column equilibrated in 100 mM Tris-HCl, pH 8, and washed with 100 mM Tris-HCl, pH 8, followed by 10 mM Tris-HCl, pH 8. Antibodies were eluted with 100 mM glycine, pH 3, and equilibrated with 1 M Tris-HCl, pH 8. Elutions were then run through a total protein column made from *vac17Δ* lysates. To prepare the total protein column, 800 ml *vac17Δ* culture was heated at 50°C in Thorner buffer (5% SDS, 8 M urea, 100 mM Tris, pH 7, 2 mM EDTA, 5 mM β-mercaptoethanol, and 10% glycerol) and lysed with glass beads. Proteins were precipitated with acetone, resuspended in PBS/1% SDS, and applied to an Actigel ALD Ultraflow 4 column (Sterogene Bioseparations, Inc.) and then prepared according to the manufacturer's protocols. The column was washed with 0.1 M NaHCO$_3$, pH 8.5/0.5 M NaCl followed by 0.2 M glycine, pH 2.5, equilibrated with 50 mM Tris-HCl, pH 7.5, 150 mM NaCl, and 0.1% Tween-20 (TTBS) containing 0.5 M NaCl, and then washed with TTBS/0.5 M NaCl/1× protease inhibitor cocktail (Sigma-Aldrich)/40 μM chymostatin. The IgG fraction was incubated in the column overnight, and flowthrough was then applied to a Vac17 affinity column. To construct the Vac17 affinity column, recombinant His-Vac17 (97–260) was purified and applied to a Ni-NTA agarose column in PP lysis buffer, pH 7.5 (20 mM NaH$_2$PO$_4$, 0.5 M NaCl, 10 mM imidazole, and 0.05% β-mercaptoethanol). IgG was loaded onto the column and washed with TTBS/0.5M NaCl. Fractions were eluted in 0.2 M glycine, pH 2.5, and equilibrated in 0.1 M Tris base.

In vivo ubiquitylation experiments

To detect ubiquitylated Vac17, pVT102U vectors encoding Vac17-GFP and *vac17-S222A-GFP* were transformed into a *vac17Δ* or *dma1Δ dma2Δ vac17Δ* mutant strain. A plasmid encoding Myc-ubiquitin driven by a CUP1 promoter and the pRS413-*myo2-D1297N* plasmid were cotransformed into the same strain. Myc-ubiquitin expression was induced with 100 μM CuCl$_2$. GFP fusion proteins were immunoprecipitated as described in the Immunoprecipitation experiments section and analyzed via immunoblotting using rabbit anti-GFP (Abcam) and rabbit anti-myc antibodies (1:2,000; Cell Signaling Technology).

In vitro kinase experiments

Expression of 6×HIS-Vac17 (97–355) and 6×HIS-*vac17-S222A* (97–355) peptides in BL21 star DE3 cells was induced with 0.2 mM IPTG (Denville Scientific) at 16°C overnight. Cells were resuspended in lysis buffer (50 mM sodium phosphate, pH 8.0, 300 mM NaCl, 10 mM imidazole, 1 mM Pefabloc [Sigma-Aldrich], and cOmplete EDTA-free protease inhibitor cocktail [Roche]) and lysed via sonication. Lysates were clarified via centrifugation at 20,000 *g* for 30 min at 4°C and incubated with Ni-NTA beads at 4°C with agitation. Immobilized HIS-tagged peptides were washed with 50 mM sodium phosphate, pH 8.0, 300 mM NaCl, and 50 mM imidazole and then eluted in 50 mM sodium phosphate, pH 8.0, 300 mM NaCl, and 300 mM imidazole. Eluted peptides were dialyzed in 50 mM Tris,

pH 8.0, and 50 mM NaCl overnight at 4°C. GST-Cla4 and *GST-cla4-k594A* were expressed in BL21 star DE3 cells via induction with 0.2 mM IPTG at 20°C for 3 h. Cells were resuspended in lysis buffer (50 mM sodium phosphate, pH 7.4, 125 mM NaCl, 10% glycerol, 2 mM MgCl$_2$, 0.1% Tween-20, 1 mM DTT, 1 mM Pefabloc, and cOmplete EDTA-free protease inhibitor cocktail) and then lysed via sonication. Clarified lysates were incubated with glutathione sepharose beads (GE Healthcare). Immobilized GST fusion proteins were washed with wash buffer (50 mM sodium phosphate, pH 7.4, 300 mM NaCl, 10% glycerol, 2 mM MgCl$_2$, 0.1% Tween-20, and 1 mM DTT) and then were washed with kinase buffer (50 mM Tris, pH 8.0, 1 mM EGTA, 2 mM MgCl$_2$, and 1 mM DTT). GST fusion proteins were eluted in 500 μl kinase buffer containing 30 mM reduced glutathione. Recombinant proteins were then purified on a size exclusion column (HiLoad 16/60 Superdex 200; GE Healthcare). In vitro kinase assays were performed using kinase buffer containing 0.5 μg kinase, 2 μg substrate, 10 mM ATP, and 50 mM β-glycerophosphate in a volume of 50 μl and then incubated at 30°C for 1 h. Kinase reactions were terminated via the addition of sample buffer and then heated at 75°C for 10 min. Proteins were resolved via SDS-PAGE and analyzed by Gelcode blue staining (Thermo Fisher Scientific) and immunoblot.

In vitro binding experiments

GST and GST fusion proteins were expressed in BL21 star DE3 cells via induction with 0.1 mM IPTG at 16°C overnight. Cells were lysed, and GST fusion proteins were immobilized on glutathione beads as described in the In vitro kinase experiments section. Immobilized proteins were washed once with yeast lysis buffer (50 mM Hepes-KOH, pH 7.6, 150 mM KCl, 1 mM EDTA, 0.5% octylglucoside, and 10% glycerol). Yeast cells grown in yeast extract peptone dextrose at 24°C were resuspended in lysis buffer containing 20 mM sodium pyrophosphate, 10 mM NaN$_3$, 20 mM NaF, 1 mM Na$_3$VO$_4$, 100 mM β-glycerophosphate, 1× protease inhibitor cocktail (Sigma-Aldrich), and cOmplete EDTA-free protease inhibitor cocktail and lysed with glass beads. GST- and GST fusion protein–bound beads were incubated with clarified yeast cell extracts for 1 h at 4°C with agitation. Beads were then washed with lysis buffer. Bound proteins were analyzed via SDS-PAGE, Gelcode blue staining, and immunoblotting. For input (6.25%), 20 μl lysate was resuspended in 20 μl sample buffer, and 5 μl was loaded into the gel.

α-Factor cell synchronization

100 ml cells (OD, 0.2–0.4) were incubated in 2.5 μM α-factor (Zymo Research) for 2–3 h until 80% of cells were arrested in G1. Cells were washed in fresh media twice to remove α-factor. 1-ml aliquots were collected every 10 min for live-cell imaging, and images were taken within 5 min of collection.

Microscopy

To visualize vacuoles, cells were labeled with either (A) 12 μg FM4-64 in 250 μl media for 1 h and then washed twice and grown in 5 ml fresh media for one doubling time (2–3 h) or (B) 100 μM 7-amino-chloromethylcoumarin (Thermo Fisher Scientific) for 30 min and then washed twice in fresh media. Live-cell images were obtained on a DeltaVision Restoration system (Applied Precision Ltd.) using an inverted epifluorescence microscope (IX-71; Olympus) with a charge-coupled device camera (CoolSNAP HQ; Photometrics) and processed in Photoshop (Adobe) and FIJI (ImageJ; National Institutes of Health).

Time-lapse microscopy

Glass-bottomed chambers (Lab-Tek II; Thermo Fischer Scientific) were treated overnight at 4°C with concanavalin A dissolved at 1 mg/ml in

50 mM Hepes, pH 7.5, 20 mM calcium acetate, and 1 mM manganese sulfate and then washed with water and air dried for 30 min. Cells adsorbed to concanavalin A–treated chambers for 2 min. Unbound cells were removed by aspiration, and 250 µl fresh media was added. Time-lapse microscopy was performed at 2-min intervals using an inverted microscope (T*i*-U; Nikon) with an iXon DV897 camera (Andor) with a 100× 1.4 NA oil immersion objective, a light engine (Lumencore), and a GFP/mCherry dual-band filter set (Chroma Technology Corp.).

Online supplemental material

Fig. S1 shows how deletion of Ste20 or Cla4 causes a partial defect in the termination of vacuole transport. Fig. S2 shows how Cla4 localizes to the vacuole after the vacuole contacts the bud cortex. Fig. S3 shows how Cla4 colocalizes with Vac17 and the vacuole at the bud cortex. Video 1 shows how Vac17-GFP disappears and the vacuole remains in the center of the cell. Video 2 shows how *vac17-S222A-GFP* and the vacuole persist at the bud cortex before moving to the mother-bud neck. Table S1 is a list of the yeast strains used in this study. Table S2 is a list of the plasmids used in this study.

References

Bartholomew, C.R., and C.F. Hardy. 2009. p21-activated kinases Cla4 and Ste20 regulate vacuole inheritance in *Saccharomyces cerevisiae*. *Eukaryot. Cell.* 8:560–572. http://dx.doi.org/10.1128/EC.00111-08

Boyce, K.J., and A. Andrianopoulos. 2011. Ste20-related kinases: effectors of signaling and morphogenesis in fungi. *Trends Microbiol.* 19:400–410. http://dx.doi.org/10.1016/j.tim.2011.04.006

Cvrcková, F., C. De Virgilio, E. Manser, J.R. Pringle, and K. Nasmyth. 1995. Ste20-like protein kinases are required for normal localization of cell growth and for cytokinesis in budding yeast. *Genes Dev.* 9:1817–1830. http://dx.doi.org/10.1101/gad.9.15.1817

Eves, P.T., Y. Jin, M. Brunner, and L.S. Weisman. 2012. Overlap of cargo binding sites on myosin V coordinates the inheritance of diverse cargoes. *J. Cell Biol.* 198:69–85. http://dx.doi.org/10.1083/jcb.201201024

Govindan, B., R. Bowser, and P. Novick. 1995. The role of Myo2, a yeast class V myosin, in vesicular transport. *J. Cell Biol.* 128:1055–1068. http://dx.doi.org/10.1083/jcb.128.6.1055

Holly, S.P., and K.J. Blumer. 1999. PAK-family kinases regulate cell and actin polarization throughout the cell cycle of *Saccharomyces cerevisiae*. *J. Cell Biol.* 147:845–856. http://dx.doi.org/10.1083/jcb.147.4.845

Ishikawa, K., N.L. Catlett, J.L. Novak, F. Tang, J.J. Nau, and L.S. Weisman. 2003. Identification of an organelle-specific myosin V receptor. *J. Cell Biol.* 160:887–897. http://dx.doi.org/10.1083/jcb.200210139

Knoblach, B., and R.A. Rachubinski. 2016. How peroxisomes partition between cells. A story of yeast, mammals and filamentous fungi. *Curr. Opin. Cell Biol.* 41:73–80. http://dx.doi.org/10.1016/j.ceb.2016.04.004

Kumar, A., P.R. Molli, S.B. Pakala, T.M. Bui Nguyen, S.K. Rayala, and R. Kumar. 2009. PAK thread from amoeba to mammals. *J. Cell. Biochem.* 107:579–585. http://dx.doi.org/10.1002/jcb.22159

Martín, H., A. Mendoza, J.M. Rodríguez-Pachón, M. Molina, and C. Nombela. 1997. Characterization of *SKM1*, a *Saccharomyces cerevisiae* gene encoding a novel Ste20/PAK-like protein kinase. *Mol. Microbiol.* 23:431–444. http://dx.doi.org/10.1046/j.1365-2958.1997.d01-1870.x

Mok, J., P.M. Kim, H.Y. Lam, S. Piccirillo, X. Zhou, G.R. Jeschke, D.L. Sheridan, S.A. Parker, V. Desai, M. Jwa, et al. 2010. Deciphering protein kinase specificity through large-scale analysis of yeast phosphorylation site motifs. *Sci. Signal.* 3:ra12. http://dx.doi.org/10.1126/scisignal.2000482

Peng, Y., and L.S. Weisman. 2008. The cyclin-dependent kinase Cdk1 directly regulates vacuole inheritance. *Dev. Cell.* 15:478–485. http://dx.doi.org/10.1016/j.devcel.2008.07.007

Peter, M., A.M. Neiman, H.O. Park, M. van Lohuizen, and I. Herskowitz. 1996. Functional analysis of the interaction between the small GTP binding protein Cdc42 and the Ste20 protein kinase in yeast. *EMBO J.* 15:7046–7059.

Pruyne, D.W., D.H. Schott, and A. Bretscher. 1998. Tropomyosin-containing actin cables direct the Myo2p-dependent polarized delivery of secretory vesicles in budding yeast. *J. Cell Biol.* 143:1931–1945. http://dx.doi.org/10.1083/jcb.143.7.1931

Schott, D., J. Ho, D. Pruyne, and A. Bretscher. 1999. The COOH-terminal domain of Myo2p, a yeast myosin V, has a direct role in secretory vesicle targeting. *J. Cell Biol.* 147:791–808. http://dx.doi.org/10.1083/jcb.147.4.791

Takahashi, S., and P.M. Pryciak. 2007. Identification of novel membrane-binding domains in multiple yeast Cdc42 effectors. *Mol. Biol. Cell.* 18:4945–4956. http://dx.doi.org/10.1091/mbc.E07-07-0676

Tang, F., E.J. Kauffman, J.L. Novak, J.J. Nau, N.L. Catlett, and L.S. Weisman. 2003. Regulated degradation of a class V myosin receptor directs movement of the yeast vacuole. *Nature.* 422:87–92. http://dx.doi.org/10.1038/nature01453

Tatebayashi, K., K. Yamamoto, K. Tanaka, T. Tomida, T. Maruoka, E. Kasukawa, and H. Saito. 2006. Adaptor functions of Cdc42, Ste50, and Sho1 in the yeast osmoregulatory HOG MAPK pathway. *EMBO J.* 25:3033–3044. http://dx.doi.org/10.1038/sj.emboj.7601192

Versele, M., and J. Thorner. 2004. Septin collar formation in budding yeast requires GTP binding and direct phosphorylation by the PAK, Cla4. *J. Cell Biol.* 164:701–715. http://dx.doi.org/10.1083/jcb.200312070

Weisman, L.S. 2006. Organelles on the move: insights from yeast vacuole inheritance. *Nat. Rev. Mol. Cell Biol.* 7:243–252. http://dx.doi.org/10.1038/nrm1892

Westermann, B. 2014. Mitochondrial inheritance in yeast. *Biochim. Biophys. Acta.* 1837:1039–1046. http://dx.doi.org/10.1016/j.bbabio.2013.10.005

Wu, C., S.F. Lee, E. Furmaniak-Kazmierczak, G.P. Côté, D.Y. Thomas, and E. Leberer. 1996. Activation of myosin-I by members of the Ste20p protein kinase family. *J. Biol. Chem.* 271:31787–31790. http://dx.doi.org/10.1074/jbc.271.50.31787

Yau, R.G., Y. Peng, R.R. Valiathan, S.R. Birkeland, T.E. Wilson, and L.S. Weisman. 2014. Release from myosin V via regulated recruitment of an E3 ubiquitin ligase controls organelle localization. *Dev. Cell.* 28:520–533. http://dx.doi.org/10.1016/j.devcel.2014.02.001